Available online at www.sciencedirect.com

SciVerse ScienceDirect

Ceramics International 38 (2012) 1717–1724

CERAMICS INTERNATIONAL

www.elsevier.com/locate/ceramint

Short communication

Nanostructured cementitious sol gel coating on graphite for application in monolithic refractory composites

S. Mukhopadhyay *, G. Das, I. Biswas

Ceramic Engg. Section, Department of Chemical Technology, Calcutta University, 92 APC Road, Kolkata 700009, India

Received 1 July 2011; received in revised form 25 August 2011; accepted 1 September 2011
Available online 8 September 2011

Abstract

A nanostructured sol gel coating of calcium aluminate ($CaAl_2O_4$) over flaky graphite has been prepared by a hybrid set of precursors. X-ray diffraction (XRD), Fourier transformed infrared spectroscopy (FTIR), differential thermal analysis (DTA), particle size distribution and microstructural studies have been performed to understand the phase evolution of calcium aluminate and its related characteristics. The topography and microstructural aspects of coated and uncoated graphites have been differentiated by atomic force microscopy (AFM) and scanning electron microscopy (SEM) with energy dispersive spectral (EDS) analysis. FTIR and XRD patterns of both graphites have also been investigated to substantiate the evolution of a thin extended hydrophilic film of calcium aluminate over coated ones. The better oxidation resistance of coated graphite has been confirmed by thermogravimetric analysis (TGA). Improved water-wettability of coated graphites has been examined by the 'ball-in-hand' test for moisture requirement during installation of a high alumina based refractory castable composite containing that graphite. Green bulk density of castable cubes has been determined to corroborate the better performance of the graphite coated with calcium aluminate.

Keywords: A. Sol–gel processes; B. Electron microscopy; D. Carbon; E. Refractories; $CaAl_2O_4$

1. Introduction

Carbon containing refractories have ubiquitous contributions towards preshaped and unshaped products used in both ferrous and non-ferrous industries. A lot of research is being done, especially on the development of carbon containing high alumina castables. However poor water-wettability and significant loss of carbon in furnace atmosphere pose two major impediments towards their commercial realization. Several attempts are thus being taken to incorporate carbon/graphite into castable matrix in a tricky and ingenious way to circumvent those drawbacks [1–5]. We have undertaken a modified sol gel method for surface treatment of graphite in a moderately cost-effective way [6–8]. It may enable the refractory makers to utilize that graphite in castables with noticeable improvement in performance [9,10].

Versatile research on the performance of new generation monolithic refractories brought a strategic interest to unfold the characteristics of castable matrices. Nowadays, refractory castables are considered as composite materials [11], composed of refractory aggregates, microphase bond materials and ultrafine oxide/non-oxide additives. Among other constituents, quality and quantity of calcium aluminate cement in matrix gave rise to a number of refractory products classified as low cement, ultra low cement and no cement castables. As such, this calcium aluminate cement, the most common bond system exerted a critical role in castable forming as well as in developing its high temperature performance. The vital ingredient of this refractory binder is calcium monoaluminate ($CaAl_2O_4$). Similar to other cementitious materials, Ca^{2+} and Al^{3+} ions in presence of water, form needle-shaped hydrates that set and harden the castable structure by restraining the displacement of refractory particles. Courses of hydration reactions of calcium aluminates have been well established [12]. The conventional method of processing calcium aluminate compound by solid state reaction is very lengthy requiring a temperature above 1400 °C. Owing to this, a parallel set of chemical processing routes have also been explored [13–18].

Similar to our previous work [6–10], we adopted here the sol gel synthesis of calcium aluminate precursor to conveniently

* Corresponding author.
E-mail address: msunanda_cct@yahoo.co.in (S. Mukhopadhyay).

0272-8842/$36.00
doi:10.1016/j.ceramint.2011.09.006

coat graphite surface at a significantly lower temperature. Polymeric sol is always preferred for thin film making [19,20], due to its more extended structure with an all-pervasive network. It reduces pore size and provides exceptional chemical homogeneity. But its cost may not be commercially acceptable for refractory applications. Therefore we attempted to tie up between the price factor and the coating quality by synthesizing a thin film of calcium aluminate via so called hybrid precursors, i.e., one from alkoxide origin and the other from a cheaper nitrate origin. This calcium aluminate coated graphite should be well compatible to the cement-containing castable matrix to retain graphite in the structure for an extended period. It should also enhance the water-wettability and oxidation resistance of graphite underneath the coating. Last but not the least, coating on graphite will provide a substantial opportunity to reduce CO_2 emissions in refractories used for iron and steel industries. This should improve overall energy efficiency and control atmospheric pollution. The present contribution has been focused to the synthesis and characterization of calcium monoaluminate by sol gel route to coat refractory grade flaky graphites. Its possible application in a high alumina based castable has also been touched upon, however, the detailed castable performance will be discussed in the next part of this work.

2. Experimental

The precursor sol for calcium aluminate was prepared by hybrid polymeric route, keeping the commercial point in mind. Thus one ingredient of the sol had been taken from the alkoxide ($Al(OBu^s)_3$, i.e., aluminium-sec-butoxide) origin whereas the other was from a cheaper origin, namely hydrated calcium nitrate. The other associated reagents for binary sol preparation were propanol, acetylacetone (chelating agent), deionised water, acetic and nitric acids. Stoichiometric calcium nitrate was added to boehmite sol to prepare calcium–monoaluminate gel as outlined in our previous papers [6–8]. The binary sol was subjected to dynamic light scattering (DLS) test to understand the particle size range of the thin coating to be developed over graphite surface. It was done in Malvern instrument (DTS Ver. 500) MAL 1010871 and model BI 200 SM-Goniometer (Ver.2.0), Melles Griot Hene-LASER Terbo correlator. The thermal evolution of calcium aluminate crystalline phases from the respective gel was determined by XRD and FTIR studies. For FTIR studies, the KBr pellet method was adopted using a Perkin Elmer model. For XRD analysis a 'Philips Analytical Instrument' was used with a Ni-filtered CuKα radiation at 40 kV/20 mA. DTA of calcium aluminate gel was examined to substantiate the XRD patterns. It was carried out in a Shimadzu instrument (DT-40 model) in air at a rate of 10 °C/min. For microstructural study of calcium aluminate gel powder, SEM experiment was conducted with the instruments (model) JEOL JSM 5200 and Hitachi S-3400N.

The XRD pattern of as-received flaky graphite, containing 97% fixed carbon (rest part being ash and volatile matters), was also studied. Using magnetic stirrer (REMI) and a digital ultrasonic bath (Takashi), supplied graphite was very slowly mixed to the precursor sol to form calcium aluminate coated graphite. The procedure was the same as had been described in our previous communications [6–8]. After requisite drying and sieving, the calcined mass (600 °C) was ready for incorporation in a monolithic refractory composite. The solid content of the thin coating over graphite was 1.7 wt%. The characteristics of both coated and uncoated graphites were compared by XRD, FTIR, AFM, and SEM (with EDS) studies. The AFM surface topography was examined by the instrument NANOSCOPE (R) IIIa, Version 5.3 (2005), Veeco instruments Ltd., with a scan rate 1.2 Hz and scan range 1 μm by tapping mode operation. The oxidation resistance of coated graphite was determined by TGA in the instrument (model) STA 409 C at a rate of 10 °C/min in air. The water-wettability of coated graphite was confirmed by the last part of this work given below.

The next important part was to compare the physical properties of a high alumina based castable composite containing 5.0 wt% coated (code: C+) and uncoated (code: C−) graphites, added separately to the same refractory batch. The castable was a low cement (4.0%) formulation with white fused alumina aggregates (72%) in several grades. The remainder part (24%) was also the same as discussed in our last publications [7–9], i.e., aluminium powder, micronized alumina, sodium hexametaphosphate, microsilica and spinel fines. The preparation of castable cubes (25 mm) included dry and wet mixing of ingredients before casting in moulds. Water was added to both 'C+' and 'C−' castables to achieve a suitable flow-value appropriate for installation (ASTM C 230). ASTM C 860-00 (2005) was also followed to note the difference in the requirement of casting water in both 'C+' and 'C−'. It was similar to the 'ball-in-hand' test performed by preparing a compact ball of wet castable mix in hands. The rounded monolithic lump was thrown in air in vertical direction up to a certain height and caught subsequently. The lump retained its cohesive nature at a certain water content that indicated its proper consistency; below this limit the mix crumbled into pieces, while above this it started seeping readily through the fingers. Both the samples were then cured in humid condition for 24 h, followed by air drying (24 h) and oven drying at 110 °C (72 h). The green bulk density (BD) of the samples was determined by standard method (ASTM C 20-00), taking the average of four specimens.

3. Results and discussion

Fig. 1a confirms that the particles in precursor sol are well below 60 nm and a significant volume fraction is below 10 nm; these finer nanoparticles should definitely react to generate calcium aluminate phases at significantly lower temperature. Owing to the release of a large amount of fugitives present in gel, the loss in weight of the gel is more than 65% up to 1000 °C as obtained from the TGA report (not shown here).

It is suggested that the pyrolysis of the chelated alkoxide-derived gel $[Al(OBu^s)_{3-x}(AcAc)_x]$and vapourisation of acetylacetone (AcAc) proceed via an auto-combustion process at a lower temperature range [17]. A broad endotherm (Fig. 1b) at 100 °C is due to loss of adsorbed water and removal of other

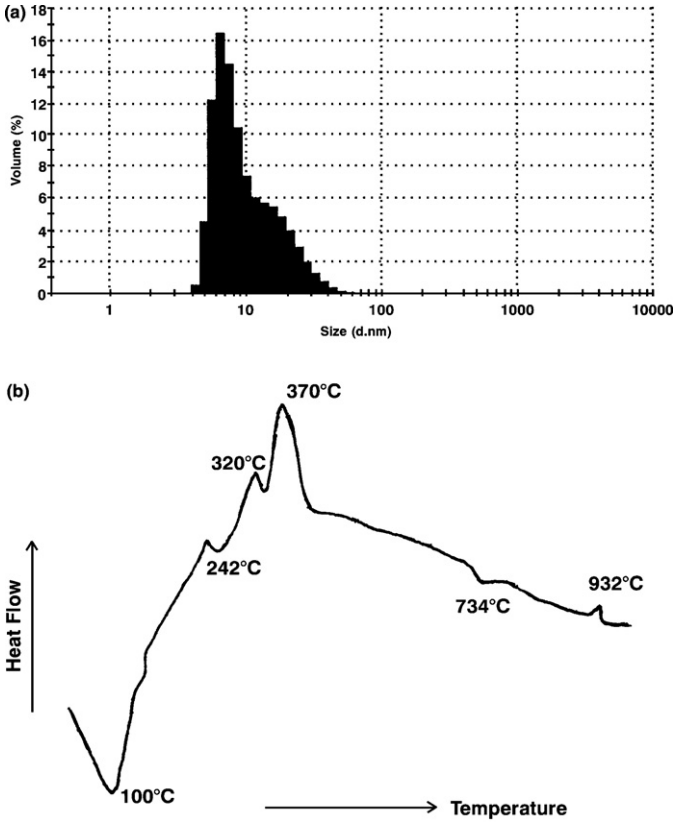

Fig. 1. (a) Particle size distribution of the precursor sol of calcium aluminate, and (b) differential thermal analysis of calcium aluminate gel powder.

volatiles. The exotherm at ~242 °C can be due to the onset of decomposition of adherent nitrates in the gel. Adjacent small endotherms indicate the loss of organic solvent and elimination of bonded water. The exotherm above 320 °C can be associated with the oxidation of residual organic materials (e.g., butanoic acid) [6]. Decomposition of hydroxides and conversion of boehmite to gamma alumina phase starts before 370 °C as evident from the endothermic peak. Between 450 and 750 °C, the TGA of the gel (not displayed here) showed some loss that could be attributed to removal of any unreacted nitrates [13,14]. Some authors suggested crystallization of $12CaO{\cdot}7Al_2O_3$ at 700 °C from a similar gel [13], and formation of multiple aluminates before resulting in calcium monoaluminate as the major phase [17]. Beyond this temperature, the weight loss is significantly low. It is suggested that γ-Al_2O_3 and CaO start forming calcium aluminates nearby 930 °C as confirmed by the last small peak. It is believed that spinel type $CaAl_2O_4$ compound is the main crystalline phase (orthorhombic/pseudo-hexagonal) [21], although some $CaAl_4O_7$ and transition alumina phases coexist as corroborated later in XRD plots. It has been documented that the formation of spinel-type $CaAl_2O_4$ (and $CaAl_4O_7$) at lower temperature is favoured by γ-Al_2O_3 [22]. Thus crystallization of chemically prepared orthorhombic $CaAl_2O_4$ is possible via defective spinel structure of Ca-doped γ-Al_2O_3 solid solution [23]. We suggest, this kind of evaporative decomposition and subsequent crystallization is more favoured by sol gel routed amorphous calcium aluminate

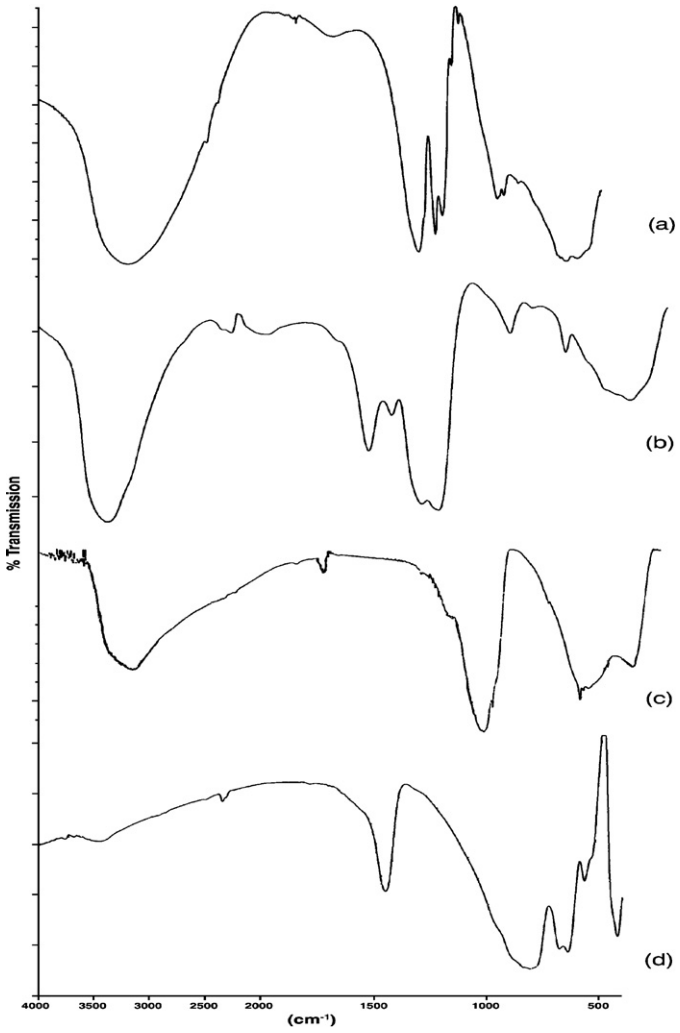

Fig. 2. FTIR patterns of (a) dried boehmite gel (80 °C) and calcium aluminate gel with increasing temperatures (b) 80 °C, (c) 500 °C and (d) 930 °C.

gel at relatively lower temperature, being assisted by auto-combustion type reaction.

Fig. 2 shows the FTIR patterns of dried boehmite gel (80 °C), and precursor calcium aluminate gel changing with thermal treatment. As the precursor of calcium aluminate gel has been prepared from alumina (boehmite) sol synthesized via Al-sec-butoxide (and then adding calcium nitrate to it), it appears quite likely that the FTIR plots of both alumina and calcium aluminate gels (Fig. 2a and b) should retain some similarities. The bands at 3400 and 1640 cm^{-1} are assigned to the deformation and stretching of molecular water and hydroxyl groups. The intensity of these bands is reduced when the gel is progressively calcined (Fig. 2c and d). Fig. 2a and b also reveal a weak band near 2500 cm^{-1} due to organic groups pertinent to the alkoxide precursor $Al(OBu^s)_3$ [13]. The band centered around 1440 cm^{-1} may be attributed to vibration of carbonate groups due to formation of $CaCO_3$ by reactive CaO present over the coating after reaction with atmospheric CO_2 [24]. Another band at the vicinity of 1360 cm^{-1} in both the gels indicates the Al=O linkage reported before [8], although nitrate motions could also be

associated with it [13]. The peak nearby 820 cm^{-1} in calcium aluminate gel can be ascribed to $Ca(NO_3)_2$ [13]. The band centered around 1060 cm^{-1} in both of those gels is ascribed to Al–OH bending [8,25]. The less sharp bands between 560 and 700 cm^{-1} in boehmite gel are due to formation of AlO_6 groups. It converts later to the Ca–O–Al linkage in calcium aluminate gel, corresponding to the formation of spinel-type compound. It is known that N–O bend in nitrates is at 810–840 cm^{-1} whereas carbonates are at 860–880 cm^{-1}. Bands at around 1500–1550 cm^{-1} can also be ascribed due to CO_2 or NO_2 stretching, all of which are minimised at 930 °C (Fig. 2d). Some bands beyond 1400 cm^{-1} corresponding to the chelate formed between Al-sec-butoxide and AcAc have been overlapped with the other constituents mentioned above [17]. At 500 °C, the peak nearby 820 cm^{-1} (Fig. 2c) can be due to defective spinel type gamma alumina [26]. Spinel ($CaAl_2O_4$) formation is quite clear in the bands within 560–700 cm^{-1} in Fig. 2d. The small peak below 500 cm^{-1} is due to evolution of alpha or transition alumina phases [27], as confirmed in the XRD report.

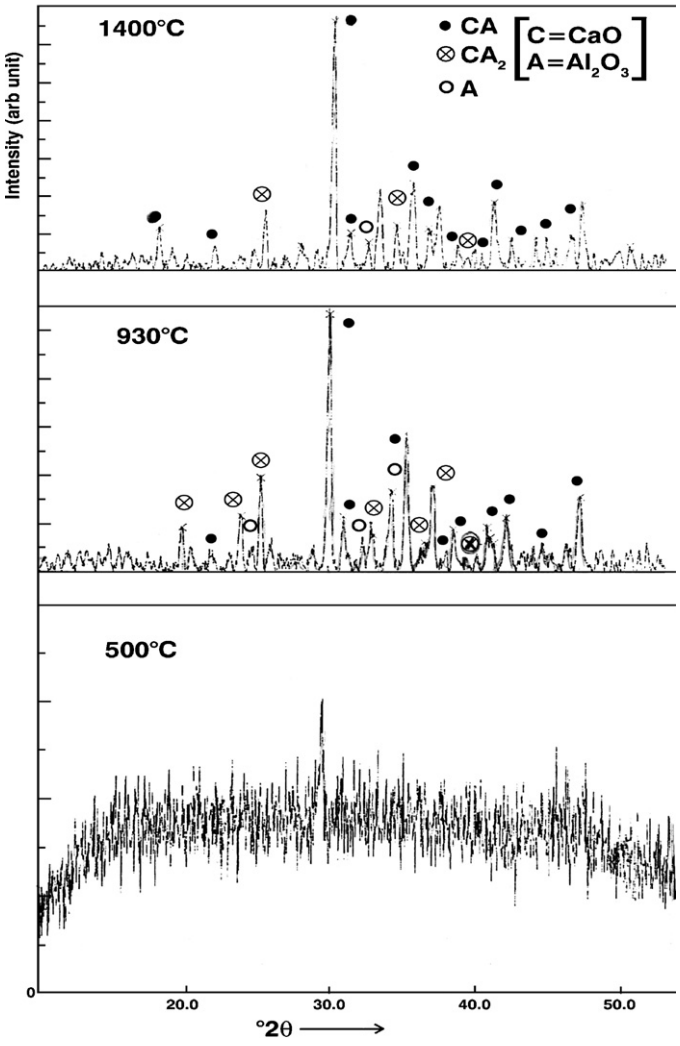

Fig. 3. Crystalline phase evolution in calcium aluminate gel with increasing temperature (500, 930 and 1400 °C).

Fig. 3 reveals the XRD patterns of calcium aluminate gel with increasing temperatures (500, 930 and 1400 °C). At 500 °C the material is predominantly amorphous [15], although some nanocrystallite formation has been indicated. As the precursor sol is boehmitic one, we suggest that the reaction here proceeds via the formation of intermediate nanocrystalline calcium-doped gamma-alumina phase. Both sol–gel and auto-combustion processes must have assisted this [17]. At 600 °C, calcium nitrate has been reported to form calcium oxide that must have reacted with gamma-alumina [23,28]. Well-crystallized monocalcium aluminate phases are obtained thereafter at 930 °C along with calcium dialuminate and minor quantity Al_2O_3 phases. At this temperature, very small additional peaks are observed that are identified as $12CaO{\cdot}7Al_2O_3$ phases (not shown in plot). Calcination up to 1400 °C promotes crystallinity of calcium monoaluminate phase and removes the minor Al_2O_3 phase [17,28].

Fig. 4 shows SEM micrographs of calcium aluminate gel heat-treated at 500 and 930 °C. As agglomeration can hardly be avoided during nanosized powder preparation by chemical route, therefore the particles in between 500 and 930 °C are observed to form the agglomerates comprised of a lot of tiny primary particles. Calcium aluminate is generated here via intermediate gamma-alumina phase; so similar morphological features are reflected in the structure at lower temperature, i.e., platelets, spherical, foil-type, ellipsoidal, etc. [8]. At higher temperature, hexagonal and elongated habits of crystals are prominent due to the crystallization of calcium aluminates with orthorhombic and pseudo-hexagonal crystallites.

Fig. 5 shows the XRD reports of coated and uncoated graphite. The flaky microstructure of as-received graphite is clear from the SEM micrograph shown inset. The XRD pattern of the as-received graphite (Fig. 5a) showed the characteristic peaks at around 27° and 55°. However, in coated graphite (Fig. 5b) fine crystallites of calcium aluminates (mainly the major peak is visible) are generated over graphite flakes, may be due to the formation of calcium doped gamma alumina phase in between 500 and 600 °C. As the onset of nanocrystalline calcium aluminate formation takes place via gamma alumina beyond 500 °C, it is obvious that the main peak of calcium monoaluminate should be present in the coated graphite calcined at 600 °C. This phase has been developed due to the high free energy of the thin precursor gel and interaction between gamma-alumina and calcium-enriched compositions in that gel. Gamma-alumina is Lewis acidic in nature, whereas CaO is well-known with its water affinity. Thus $CaAl_2O_4$ prepared via Ca-doped γ-Al_2O_3 at above 500 °C must retain its hydrophilic properties [7,29]. It becomes more pronounced when nanostructured $CaAl_2O_4$ phases are distributed over graphite surface as corroborated later in AFM results. We suggest further that the pseudo-hexagonal $CaAl_2O_4$ rich coating at 930 °C onwards must be compatible to hexagonal graphite underneath, when added to the matrix of refractory composite.

Fig. 6 represents the comparison of AFM reports of coated and uncoated graphites. The surface topography of uncoated graphite (Fig. 6a) is very smooth and roughness is virtually absent due to the lack of finer phases over graphite. In contrast,

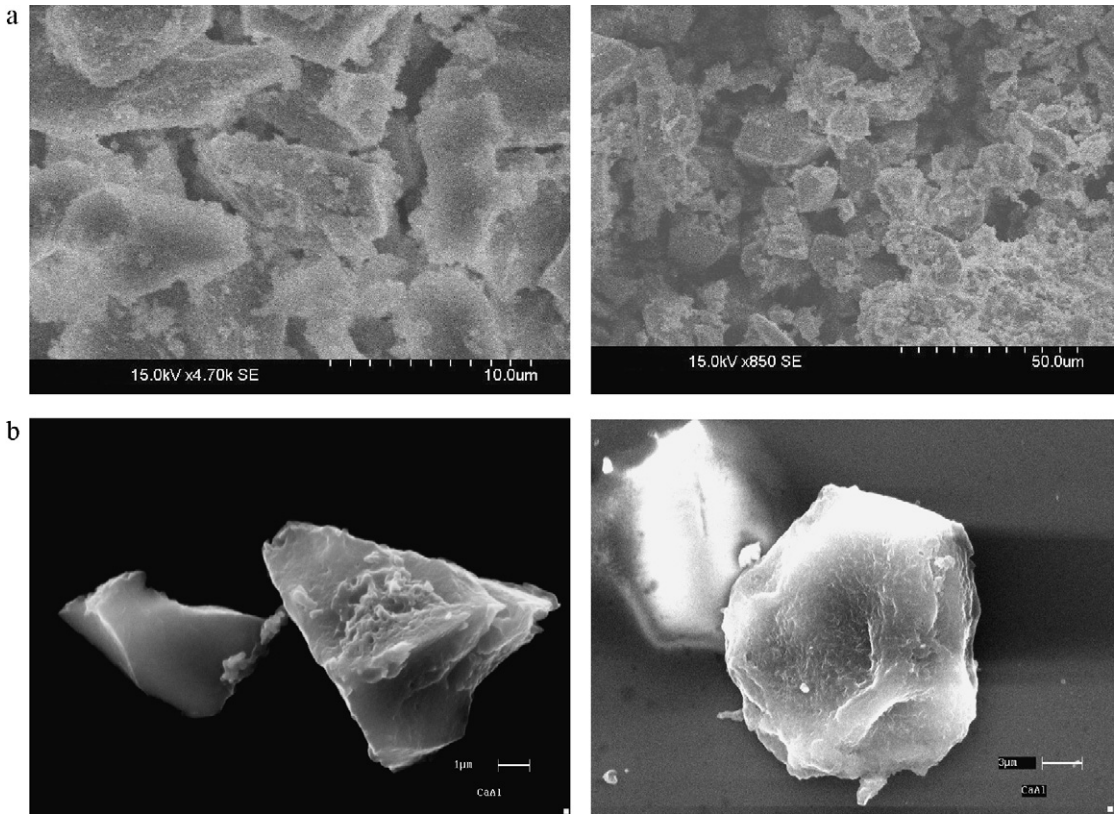

Fig. 4. SEM micrographs of calcium aluminate gel powder calcined at (a) 500 °C and (b) 930 °C.

round-shaped nanoparticles, i.e., nanostructured calcium aluminate phases are abundantly and sporadically present over the coated graphite surface (Fig. 6b, both in 2D and 3D illustrations) with sizes well below 100 nm. As such a lot of interfacial areas are generated over flaky graphite that must enhance the hydrophilicity and oxidation resistance of graphite [8]. It is well known that calcium aluminate is prone to hydration which occurs via a three-step process of dissolution, nucleation and precipitation [12]; in addition this phase has been prepared here via an intermediate gamma-alumina phase which is inherently a strong Lewis acid that readily adsorb polar molecules [6,7,29]. This twofold effect combinedly improves the water affinity of the coating. As such the coated graphites associated with a lot of chemisorbed and physisorbed hydroxyl (OH) groups, are rendered miscible to water and well incorporated into the castable matrix in due course, with less water demand.

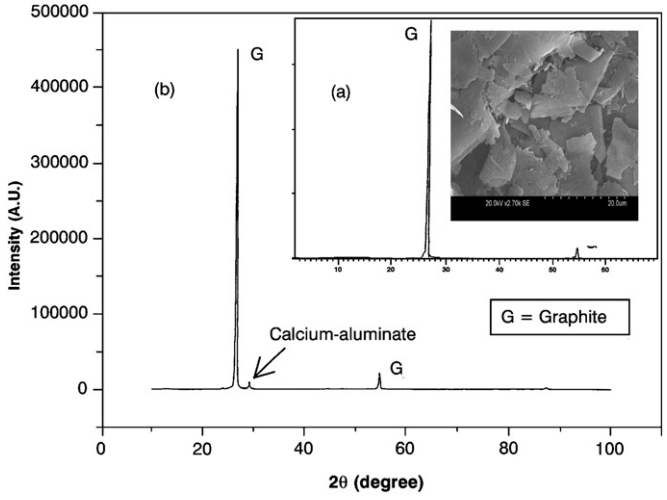

Fig. 5. XRD patterns of (a) as-received graphite (inset: SEM of as-received graphite) and (b) calcium aluminate coated graphite.

The comparison of FTIR reports of uncoated and coated graphites in Fig. 7 further confirms the results mentioned above. Fig. 7a (uncoated graphite) shows small peak at around 3437 cm^{-1} for feeble (OH) groups associated to it. The hydrophobic bands are clear at 770 cm^{-1} for (=C–H) linkage (i.e., aromatic ring structure) and at 1625 cm^{-1} for (C=C) linkage. After coating formation (Fig. 7b) the band at 770 cm^{-1} has been substantially masked [6,7]. Association of more hydrophilic groups (free and associated OH groups) are confirmed by the increased band at 3437 cm^{-1} and presence of a narrow band at 3754 cm^{-1}. The band at 1440 cm^{-1} can be due to calcite formation from atmospheric CO_2 over the calcium enriched regions of coating surface [24]; in fact the band at 2377 cm^{-1} also supplements the adherence of CO_2 over coating. The peak at 1440 cm^{-1} may also be due to Al–O stretching due to thin ceramic coating. The bands within 1670–1760 cm^{-1} (e.g., at 1720 cm^{-1}) can be assigned to (C=O)

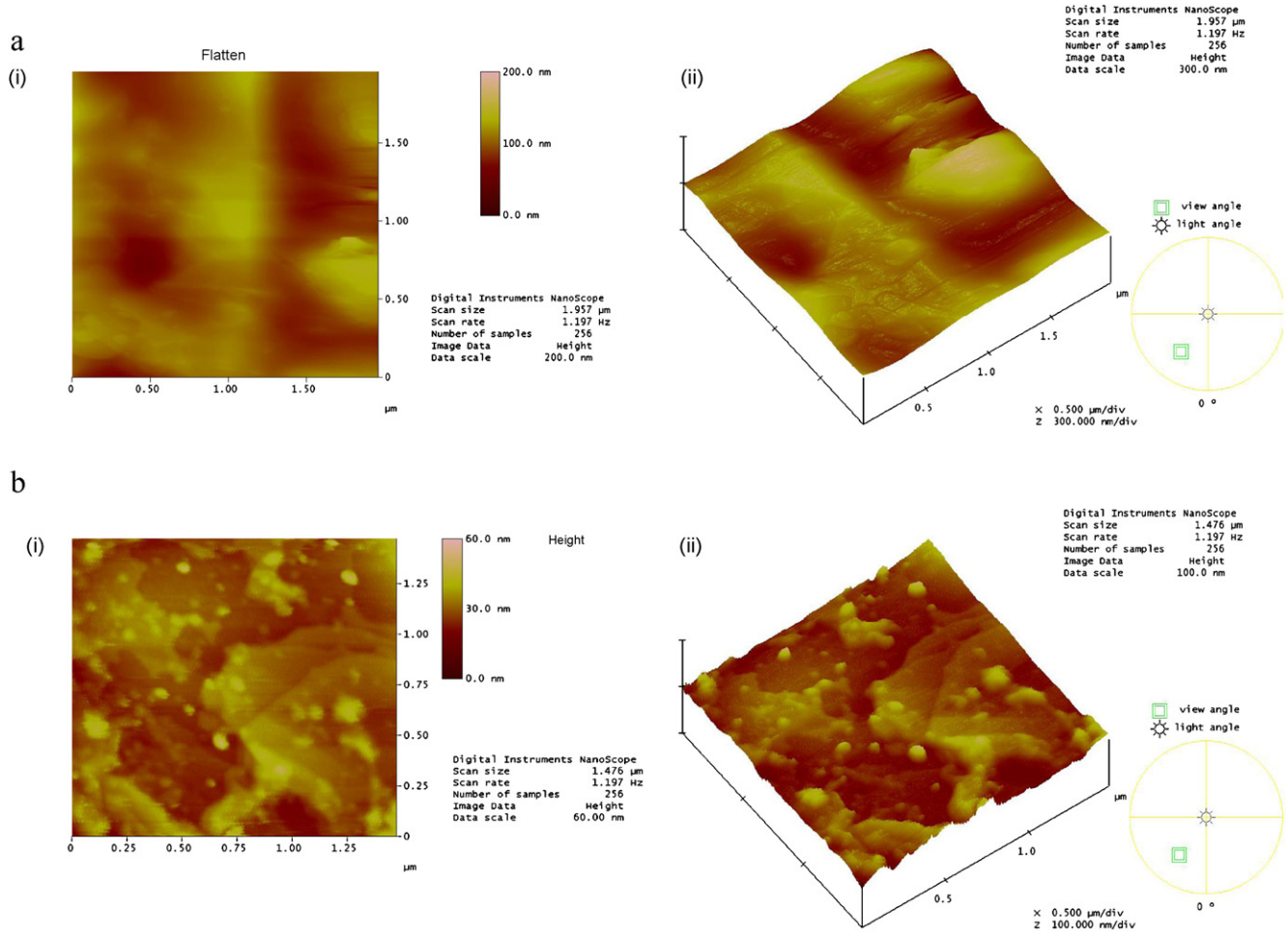

Fig. 6. AFM surface topography of (a) uncoated graphite [(i) 2D view, (ii) 3D view], and (b) calcium aluminate coated graphite [(i) 2D view, (ii) 3D view].

linkage from carboxylic group which is hydrophilic too [4]. The bands below 1260 cm^{-1} could also be due to (C–O) stretch of carboxylic group. Al–OH bending and Al–O vibration are clear from the bands nearby respectively at 1074 and 950 cm^{-1} [25]. The bands between 550 and 690 cm^{-1} are pertinent to the formation of AlO_6 groups and correspond to calcium aluminate spinel type compounds generated over the coating by sol–gel route [21]. As such the hydrophilicity of graphite is enhanced due to its surface modification by this $CaAl_2O_4$ coating. It must enhance the water-wettability of coated graphite.

In Fig. 8, the results of SEM micrograph of coated graphite have been shown along with two EDS plots associated with it. The larger plot (Fig. 8b) represents the overall/average composition of coated graphite shown in the micrograph; whereas the smaller plot (Fig. 8a) is the EDS taken at some particular points on calcium–aluminate coatings. The strong carbon peak in both the plots infers that the coating is thin enough so that the carbon underneath is visible by electron bombardment. The silicon (Si) peak of as-received graphite is prominent due to the silica-rich impurities in ash [8]; however the siliceous peak has been effectively masked by calcium (Ca) and aluminium (Al) peaks when some specific regions over the coated surface are considered. It also qualitatively confirms the elemental (1:2) stoichiometry of calcium and aluminium in the coating.

As the sol–gel derived calcium aluminate nanostructured thin film with immense surface area inhibited the contact between atmospheric oxygen and graphite surface, oxidation resistance or thermal stability of coated graphite increased manifold (Fig. 9). The TG plot of as-received graphite (inset) clearly indicates that a significant improvement took place after coating formation when graphite is treated at high temperature in oxidizing atmosphere.

Last part of this work includes the comparison of consistency and BD of castables. Ball-in-hand test (ASTM C 860-00) has been performed for evaluating the consistencies of two castables. It was observed that the uncoated graphite containing castable needed 10.8% water to mould it in the form of a compact ball in hand; i.e., the rounded lump retained its cohesive nature at 10.8% water content. Below this limit the lump disintegrated into small pieces, while above this limit the lump started seeping through the fingers. But for the castable composite mix containing calcium–aluminate coated graphite, the water-content was determined to be 7.5% to satisfy proper consistency. Coated graphite, thus, will be definitely acceptable to castable matrix (that already contains calcium aluminate

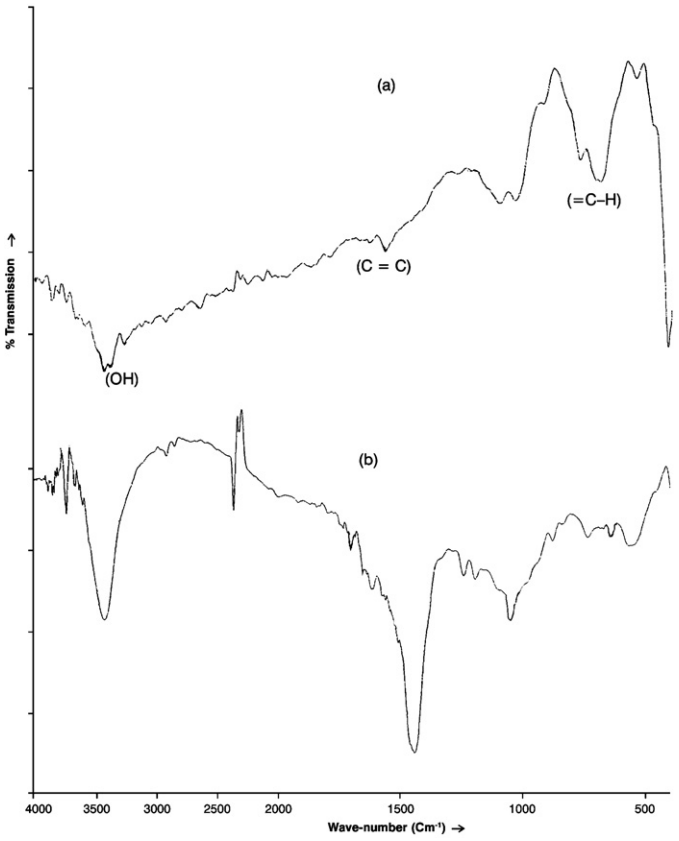

Fig. 7. FTIR patterns of (a) uncoated graphite and (b) calcium aluminate coated graphite.

cement) with less water requirement. Consequently the green B.D. (110 °C) of uncoated graphite containing castable (2.50 g/cm^3) was markedly increased to 2.83 g/cm^3 when calcium–aluminate coated graphite has been used. It should reduce the porosity of 'C+' castable that will surely improve its refractory performance [30]. The $CaAl_2O_4$ coating thus behaves as an intermediate thin ceramic layer, bridging the graphite with

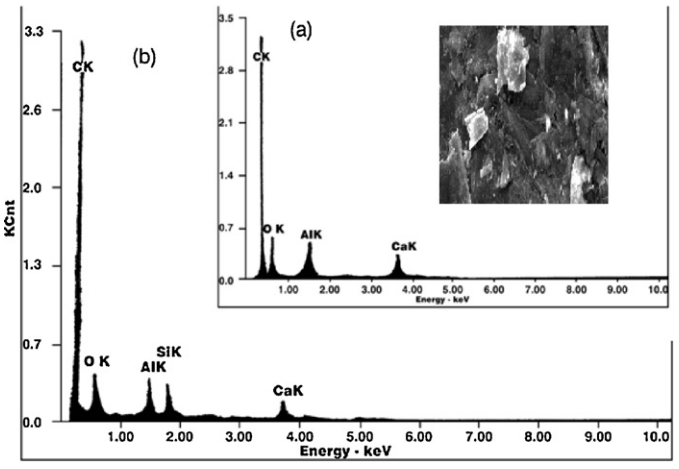

Fig. 8. EDS plots of coated graphite (a) at some specific points on coated surface (inset: SEM of coated graphite), and (b) the overall composition of graphite surface.

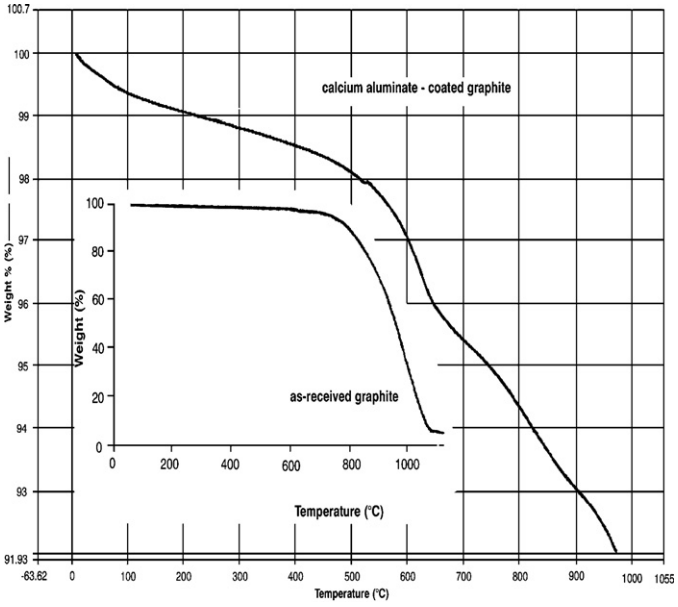

Fig. 9. TGA patterns of calcium aluminate coated graphite and uncoated graphite (inset).

oxide-enriched matrix of refractory aggregates. Depletion of graphite in furnace atmosphere is also prevented by this layer. The high temperature performance of 'C+' and 'C−' castables will be discussed in detail in the next part of our work as previously reported elsewhere [9].

4. Conclusions

From the laboratory scale investigation, it may be concluded that:

(1) Evolution of crystalline calcium aluminate ($CaAl_2O_4$) by sol gel synthesis from a hybrid set of precursors occurs at much lower temperature (above 900 °C) than the conventional process (∼1400 °C).
(2) As-received flaky graphite can be effectively coated by 1.7 wt% of those calcium aluminate precursors via formation of intermediate nanostructured calcium-doped gamma alumina after calcination at 600 °C.
(3) The better oxidation resistance of coated graphite, compared to the uncoated one, is confirmed by its significantly less weight loss after heating up to 1000 °C. The water-holding characteristics of coated graphite are corroborated by its association with more hydrophilic functional groups, e.g., (OH), due to the formation of a thin film of calcium aluminate over graphite surface.
(4) Consequently, that coated graphite, incorporated to a refractory castable, consumes much reduced water (from 10.8% to 7.5%) imparting proper consistency of the monolithic mix during fabrication. As such, the green bulk density of this high alumina based refractory is remarkably improved (2.83 g/cm^3) compared to the same composite material prepared by the uncoated graphite (2.5 g/cm^3).

References

[1] K. Sankaranarayanane, K. Balamurugan, M. Rigaud, Mechanical properties up to 1100 °C. of Al_2O_3–MgO-extruded graphite pellets castables reinforced with steel, Ceram. Int. 35 (2009) 359–363.

[2] X. Liu, Z. Wang, S. Zhang, Molten salt synthesis and characterization of titanium–carbide coated graphite flakes for refractory castable applications, Int. J. Appl. Ceram. Technol. 8 (4) (2011) 911–919.

[3] I.R. de Oliveira, A.R. Studart, F.A. de Silva Junior, V.C. Pandolfelli, Stabilization of graphite containing aqueous suspensions, Ceramica 46 (2000) 186–195.

[4] A. Saberi, F. Gollestani-Fard, M. Willert-Porado, R. Simon, T. Gerdes, H. Sarpoolaky, Improving the quality of nanocrystalline $MgAl_2O_4$ spinel coating on graphite by a prior oxidation treatment on the graphite surface, J. Eur. Ceram. Soc. 28 (2008) 2011–2017.

[5] C.G. Aneziris, S. Dudczig, Carbon containing castables and more, Adv. Sci. Technol. 70 (2010) 72–81.

[6] Sk.A. Ansar, S. Bhattacharya, S. Dutta, S.S. Ghosh, S. Mukhopadhyay, Development of mullite and spinel coatings on graphite for improved water-wettability and oxidation resistance, Ceram. Int. 36 (2010) 1837–1844.

[7] S. Mukhopadhyay, S. Dutta, S.A. Ansar, S. Das, S. Misra, Spinel-coated graphite for carbon containing refractory castables, J. Am. Ceram. Soc. 92 (8) (2009) 1895–1900.

[8] S. Mukhopadhyay, Improved sol gel spinel ($MgAl_2O_4$) coatings on graphite for application in carbon containing high alumina castables, J. Sol–Gel Sci. Technol. 56 (1) (2010) 66–74.

[9] S. Mukhopadhyay, Sk.A. Ansar, D. Paul, G. Bhowmick, S. Sengupta, Characteristics of refractory castables containing mullite and spinel coated graphites, Mater. Manuf. Process., doi:10.1080/10426914.2011.560501, in press.

[10] S. Mukhopadhyay, D. Paul, G. Bhowmick, P.K. DasPoddar, Sk.A. Ansar, Mullite coatings on graphite for application in carbon containing monolithic refractory, Ind. Ceram. 31 (2) (2011) 129–136.

[11] W.E. Lee, S. Zhang, M. Karakus, Refractories: controlled microstructure composites for extreme environments, J. Mater. Sci. 39 (2004) 6675–6685.

[12] K.L. Scrivener, A. Campas, Calcium aluminate cements, in: P.C. Hewlett (Ed.), Lea's Chemistry of Cement and Concrete, fourth ed., Butterworth-Heinemann, Oxford, 2001 , pp. 709–778 (Chapter 13).

[13] A.A. Goktas, M.C. Weinberg, Preparation and crystallization of sol–gel calcia–alumina compositions, J. Am. Ceram. Soc. 74 (5) (1991) 1066–1070.

[14] M. Uberoi, S.S. Risbud, Processing of amorphous calcium aluminate powders at <900 °C, J. Am. Ceram. Soc. 73 (6) (1990) 1768–1770.

[15] L. Kerns, M.C. Weinberg, S. Myers, R. Assink, Al coordination in sol–gel and conventional calcium aluminate glasses, J. Non-Cryst. Solids 232–234 (1998) 86–92.

[16] M.A. Gulgun, O.O. Popoola, W.M. Kriven, Chemical synthesis and characterization of calcium aluminate powders, J. Am. Ceram. Soc. 77 (2) (1994) 531–539.

[17] S. Kurajica, V. Mandic, J. Sipusic, Thermal evolution of calcium aluminate gel obtained from aluminium-sec-butoxide chelated with ethylacetoacetate, J. Ceram. Sci. Technol., doi:10.4416/JCST2010-00017.

[18] M.F. Zawrah, N.M. Khalil, Synthesis and characterization of calcium aluminate nanoceramics for new applications, Ceram. Int. 33 (8) (2007) 1419–1425.

[19] M.A. Aegerter, M. Jafelicci Jr., D.F. Souza, E.D. Zannotto, Sol Gel Science and Technology, World Scientific Publishing, Singapore, 1989, pp. 356–363.

[20] C.J. Brinker, G.W. Scherer, Sol–Gel Science: The Physics and Chemistry of Sol–Gel Processing, Academic Press Inc., San Diego, CA, 1990, pp. 239–841.

[21] J.J. Vijaya, L.J. Kennedy, G. Sekaran, K.S. Nagaraja, Utilisation of Sr(II) added calcium aluminate for the detection of volatile organic compounds, Ind. Eng. Chem. Res. 46 (19) (2007) 6251–6258.

[22] A.E. Lavat, M.C. Grasselli, E.G. Lovecchio, Effect of α and γ-polymorphs of alumina on the preparation of $MgAl_2O_4$-spinel-containing refractory cements, Ceram. Int. 36 (1) (2010) 15–21.

[23] A. Douy, M. Gervais, Crystallisation of amorphous precursors in the calcia–alumina system: a differential scanning calorimetry study, J. Am. Ceram. Soc. 83 (1) (2000) 70–76.

[24] A.F. Jimenez, P. Vazquez, A. Palomo, Effect of sodium silicate on calcium aluminate cement hydration in highly alkaline media: a microstructural characterization, J. Am. Ceram. Soc. 94 (4) (2011) 1297–1303.

[25] A. Banerjee, S. Das, S. Misra, S. Mukhopadhyay, Structural analysis of spinel ($MgAl_2O_4$) for application in spinel-bonded castables, Ceram. Int. 35 (2009) 381–390.

[26] D. Kundu, T. Manna, G. De, Preparation and characterization of thin optically transparent alumina and Ce-doped alumina, J. Sol Gel Sci. Technol. 23 (2002) 145–150.

[27] G. Urretavizcaya, A.L. Cavalieri, J.M.P. Lopez, I. Sobrados, J. Sanz, Thermal evolution of alumina prepared by the sol–gel technique, J. Mater. Synth. Process. 6 (1) (1998) 1–7.

[28] D.E. Burkes, J.J. Moore, Auto-ignition combustion synthesis of calcium aluminate ceramic powders, J. Combust. Sci. Technol. 180 (1) (2008) 143–155.

[29] Z. Zhang, T.J. Pinnavaia, Mesostructured γ-Al_2O_3 with a lathlike framework – morphology, J. Am. Chem. Soc. 124 (2002) 12294–12301.

[30] S. Banerjee, Monolithic Refractories: A Comprehensive Handbook, The American Ceramic Society, Westerville, OH, USA, 1998, pp. 56–61.